


## Charge-state distributions of relativistic gold-ion beams stripped by foils

V. P. Shevelko<sup>1,\*</sup>, N. Winckler,<sup>2</sup> and I. Yu. Tolstikhina<sup>1</sup>

<sup>1</sup>*P. N. Lebedev Physical Institute, Leninskii prospect 53, 119991 Moscow, Russia*

<sup>2</sup>*Firma ATOS, BDS R & D, 38130 Échirolles, France*

 (Received 9 October 2019; revised manuscript received 4 December 2019; published 13 January 2020)

The dynamics of charge-state fractions of relativistic gold-ion beams stripped by foils from Be to Au is investigated in the 100 MeV/u to 10 GeV/u energy range. Calculations of the fractions as a function of foil thickness are performed using the recently developed BREIT code based on the analytical solution of the balance rate equations for the ion charge-state fractions. Relativistic electron-loss and electron-capture cross sections, required for BREIT as input data, are calculated. The influence of the beam energy loss on the charge-state fractions is found to be small: less than 15%. Calculated charge-state distributions are compared with available experimental data, obtained at the GSI (Gesellschaft für Schwerionenforschung), RHIC (Relativistic Heavy Ion Collider), and BEVALAC (Bevatron Linear Accelerator) facilities, and calculations of the GLOBAL code created at GSI. The present calculations of the charge-state distributions allow one to find the optimal conditions for the maximal yield of H-like, He-like, and bare gold ions at energies considered.

DOI: [10.1103/PhysRevA.101.012704](https://doi.org/10.1103/PhysRevA.101.012704)

### I. INTRODUCTION

Stripping heavy ions in gaseous and solid targets is possible now at modern heavy-ion accelerator facilities in order to increase the projectile charge state to improve the acceleration efficiency of ion beams to higher energies. Charge-state distribution (CSD) of accelerated ions, passing through gas, solid, or plasma strippers, i.e., the dependence of ion charge-state fractions  $F_q(x)$  on the target thickness  $x$ , is one of the main characteristics, describing the interaction of projectile ions with target particles (see, e.g., [1–3]). CSD contains information about charge-state dynamics of ion beams as well as various quantities such as the mean and equilibrium charges and equilibrium thicknesses, among others. Knowledge of the  $F_q(x)$  values for a given system “ion beam + target” at fixed ion energy allows one to predict the optimal conditions (beam energy, foil material, and thickness) for the creation of ion fractions with the maximum charge and/or maximum intensity. Experimental data on the charge-state fractions of relativistic heavy multielectron ions stripped in gases and foils are rather scarce; therefore, theoretical predictions have special importance.

Fundamental experimental results on stripping relativistic heavy ions in gases and foils are presented in [4], where the CSDs were obtained at the BEVALAC accelerator (Bevatron Linear Accelerator, Lawrence Berkeley National Laboratory, Berkeley, California) and the heavy-ion synchrotron SIS/GSI (Gesellschaft für Schwerionenforschung, Darmstadt, Germany) for beams of ions from Xe to U (including Au) and targets from Be to U in the 80–1000-MeV/u energy range. Theoretical models for CSDs and the developed CHARGE and GLOBAL computer codes, which are widely used for

the investigation of relativistic heavy-ion beams, are also described in [4].

The interaction of gold-ion beams with foils was investigated at the Relativistic Heavy Ion Collider (RHIC, Brookhaven National Laboratory, Upton, New York) [5] to provide an effective yield of He-like  $\text{Au}^{77+}$  ions in the intermediate stripper at 100 MeV/u and of bare ions in the final stripper at 10 GeV/u. At 100 MeV/u, the C, Al, and combined (Al + C) strippers were used, and at 10 GeV/u one experimental point for the  $\text{Au}^{79+}$  fraction was obtained using W foil. For the interpretation of experimental data in [5], the GLOBAL code [4] was used.

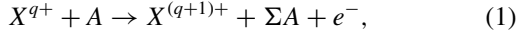
At the new Nuclotron-based Ion Collider facility (NICA project) in the Joint Institute for Nuclear Research (JINR), Dubna, Russia, an accelerator complex was created to investigate the properties of dense baryonic material [6] using ion beams from protons to bare gold ions at relativistic energies up to 4.5 GeV/u. For planning such experiments, information on the efficiency of few-hundred-MeV/u bare gold ions created after a foil in a stripping station in the output of the accelerator booster is required. For this purpose, recently [7], CSD calculations of relativistic gold ions, stripped by Cu and Au foils at 400 and 600 MeV/u, were performed, and the optimal conditions were found for the production of bare gold  $\text{Au}^{79+}$  ions with 80% and 90% probability.

The aim of this work is to investigate the charge-state distributions of relativistic gold ions, stripped by foils made from Be to Au materials in the 100-MeV/u to 10-GeV/u energy range. Equilibrium and nonequilibrium charge-state fractions are calculated using the BREIT code described in [8]. Relativistic electron-loss and electron-capture cross sections for the interaction of gold ions with the foil atoms are calculated and used as input data for BREIT. The physical properties of the CSDs, found in this work, make it possible to predict the optimal conditions to obtain the maximal yield of H-like, He-like, and bare gold ions in the energy range considered.

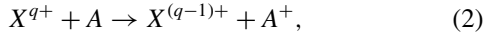
\*Shevelkovp@lebedev.ru

## II. CHARGE-CHANGING CROSS SECTIONS AND CHARGE-STATE DISTRIBUTIONS

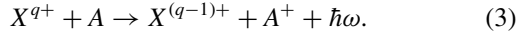
In collisions of heavy multielectron ions with foils at relativistic energies, the following single-electron processes play a key role in the interaction of the projectile ion  $X^{q+}$  of the charge  $q$  with the target atom  $A$ : (1) electron loss (EL), or projectile ionization,



(2) nonradiative electron capture (NRC),



and (3) radiative electron capture (REC), accompanied by radiation of a photon  $\hbar\omega$ ,



$\Sigma A$  in Eq. (1) means that the target atom can be excited or ionized. At relativistic energies the contribution of multiple-electron processes is usually neglected.

The total electron-capture (EC) cross section is the sum of NRC and REC cross sections:

$$\sigma_{\text{EC}} = \sigma_{\text{NRC}} + \sigma_{\text{REC}}. \quad (4)$$

At nonrelativistic energies, EL cross sections of reaction (1) decrease by the Born asymptotic law:

$$\sigma_{\text{EL}}^B \sim Z_T^2 \ln E / (q^2 E), \quad (5)$$

while in the relativistic energy domain, they have a quasiconstant behavior due to the influence of relativistic (magnetic) interaction between colliding particles [9] and are characterized by a semiempirical estimate [10]:

$$\sigma_{\text{EL}}^{\text{rel}} \sim \text{const} \sim Z_T^2 I_p^{-0.01q}. \quad (6)$$

Here  $E$  denotes the projectile energy,  $Z_T$  is the target atomic number, and  $I_p$  is the first ionization potential of the projectile.

The capture cross sections of processes (2) and (3) have the following asymptotic laws [3,11]:

$$\sigma_{\text{NRC}} \approx q^5 Z_T^5 / E^{5.5}, \quad (7)$$

$$\sigma_{\text{REC}} \approx q^4 Z_T / E^2. \quad (8)$$

The relative contribution of NRC and the REC cross sections to the sum (4) depends on the projectile energy and atomic structure of colliding particles due to different dependencies of the cross sections on atomic parameters  $q$ ,  $Z_T$ , and  $E$ . As a rule, at relativistic energies and low- $Z$  targets ( $Z_T < 30$ ), REC processes prevail, and the role of NRC is rather small, but for heavy targets (like W, Au), the contribution of NRC can be of a size comparable to REC (see [11]).

In the present paper, EL cross sections are calculated using the RICODE-M program [12] based on the relativistic Born approximation with magnetic interaction between colliding particles and relativistic wave functions for the active projectile electron in discrete and continuum spectra. The NRC cross sections are calculated by the CAPTURE code [13], and the REC values are calculated by the semiempirical Kramers formula [14] while accounting for the kinematics of colliding particles [15]. The accuracy of the present calculations of EL and EC cross sections is estimated within 30%–50%.

Calculations of CSDs of gold ions stripped by foils are performed with the BREIT code [8] based on the numerical solution of the balance rate first-order differential equations for the  $F_q(x)$  fractions [1]:

$$\frac{d}{dx} F_q(x) = \sum_{q' \neq q} F_{q'}(x) \sigma_{q'q} - F_q(x) \sum_{q' \neq q} \sigma_{qq'}, \quad (9)$$

$$\sum_q F_q(x) = 1, \quad (10)$$

where  $x$  denotes the foil thickness or the areal density of the target particles and  $\sigma_{ij}$  are one- and multiple-electron loss ( $i < j$ ) and capture ( $i > j$ ) cross sections, respectively. The equilibrium fractions  $F_q(\infty)$  correspond to the solution of the balance equations at large thicknesses, where all derivatives  $dF_q(x)/dx \rightarrow 0$ .

The BREIT code is available online with a detailed description of preparing the input files [16–18]. The energy losses of ion beams are estimated using the Atomic Interaction with Matter (ATIMA) code [19]. ATIMA is a program intended for calculating different collision characteristics of protons and heavy ions penetrating matter: stopping power, energy loss, energy-loss straggling, angular straggling, range, and mean equilibrium charge, among others.

## III. EL CROSS SECTIONS OF GOLD IONS

EL cross sections for  $\text{Au}^{q+}$  ions,  $60 \leq q \leq 78$ , colliding with neutral atoms from Be to Au at energies  $E = 10$  MeV/u to 100 GeV/u are calculated with the RICODE-M code [12] and are presented in Figs. 1 and 2 for light and heavy target atoms, respectively. EL cross sections for other ion charges can be interpolated from Figs. 1 and 2.

The two main features can be seen from Figs. 1 and 2. First, at energies  $50$  MeV/u  $\lesssim E \lesssim 400$  MeV/u, EL cross sections decrease as the Born asymptotic law (5), but as the ion energy increases, those for ions with  $q \leq 77$  become quasiconstant at  $E > 1$  GeV/u due to the relativistic interaction. The cross sections for H-like and He-like gold ions start out quasiconstant at higher energies  $E > 100$  GeV/u. Second, a big difference is seen between EL cross sections for Li- and He-like ions mainly caused by the difference in the first ionization potentials of these ions. We will see below that the difference in EL cross sections leads to a large enhancement of the nonequilibrium  $F_{77}(x)$  fraction of He-like gold ions. Calculated cross sections for ionization of gold ions by Ni ( $Z_T = 28$ ) and W ( $Z_T = 74$ ) atoms, considered further in the paper, are not shown here because these cross sections are very close (within 10%–15%) of those of Cu ( $Z_T = 29$ ) and Au ( $Z_T = 79$ ) atoms, respectively.

## IV. STRIPPING GOLD IONS AT 100 MEV/u

Nonequilibrium charge-state fractions  $F_q(x)$  of gold ions, colliding with C, Al, and double-layer (Al + C) foils at 100 MeV/u, were measured at RHIC [5]. There, for interpretation of experimental results, the GLOBAL code was used [4], intended for CSD calculations at high and relativistic energies.

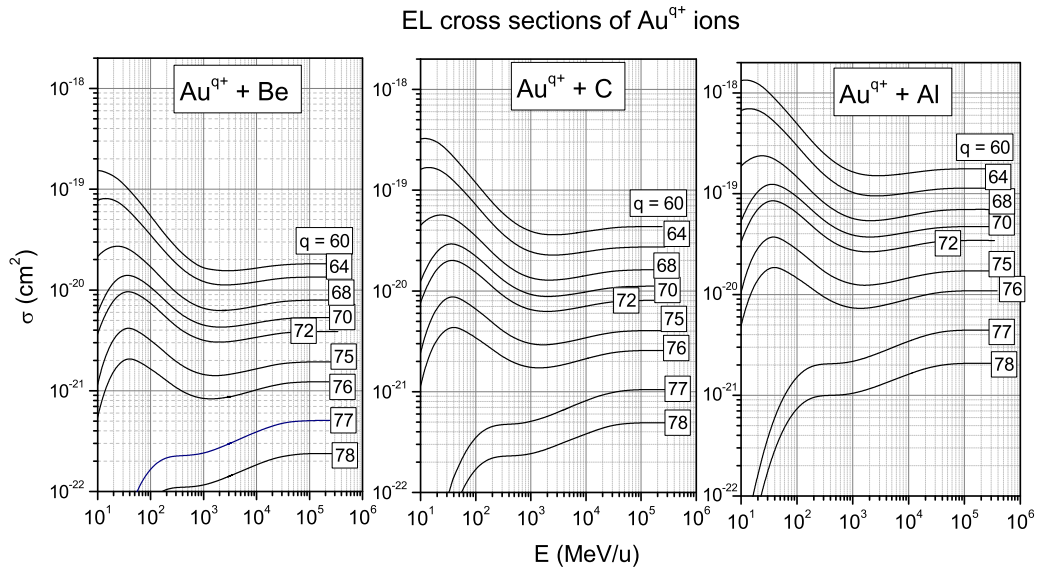


FIG. 1. Calculated EL cross sections of  $Au^{q+}$  ions,  $60 \leq q \leq 78$ , in collisions with light atoms of Be, C, and Al as a function of ion energy for the RICODE-M result.

A comparison of the present calculations with the RHIC data and GLOBAL results is shown in Figs. 3–5.

**A. C foil**

Results for stripping gold ions by the C foil are given in Fig. 3. The present calculations of EL and EC cross sections are shown in the top left graph. The top right graph presents the BREIT results for the CSD with the C foil. Calculated *equi-*

*librium thickness* for C foil  $x_{eq} = 80 \text{ mg/cm}^2$  is much larger than the thicknesses  $x = 13.9$  and  $23.1 \text{ mg/cm}^2$  used at RHIC. Experimental fractions  $F_{74} - F_{79}$  at these two thicknesses are shown in the bottom left and right graphs in comparison with the BREIT and GLOBAL calculations.

As seen from the bottom left graph of Fig. 3, the GLOBAL result for nonequilibrium gold fractions at  $x = 13.9 \text{ mg/cm}^2$  is closer to experimental data than the BREIT calculations, which, in turn, are in better agreement with experiment at a

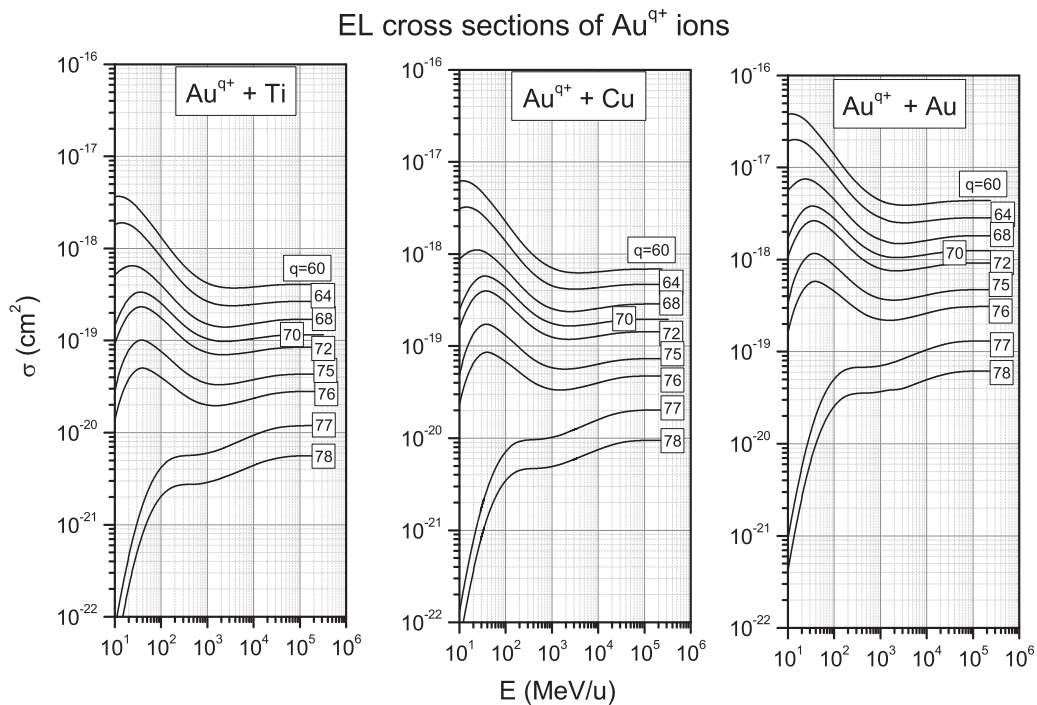


FIG. 2. Calculated EL cross sections of  $Au^{q+}$  ions,  $60 \leq q \leq 78$ , in collisions with heavy atoms of Ti, Cu, and Au as a function of ion energy for the RICODE-M result.

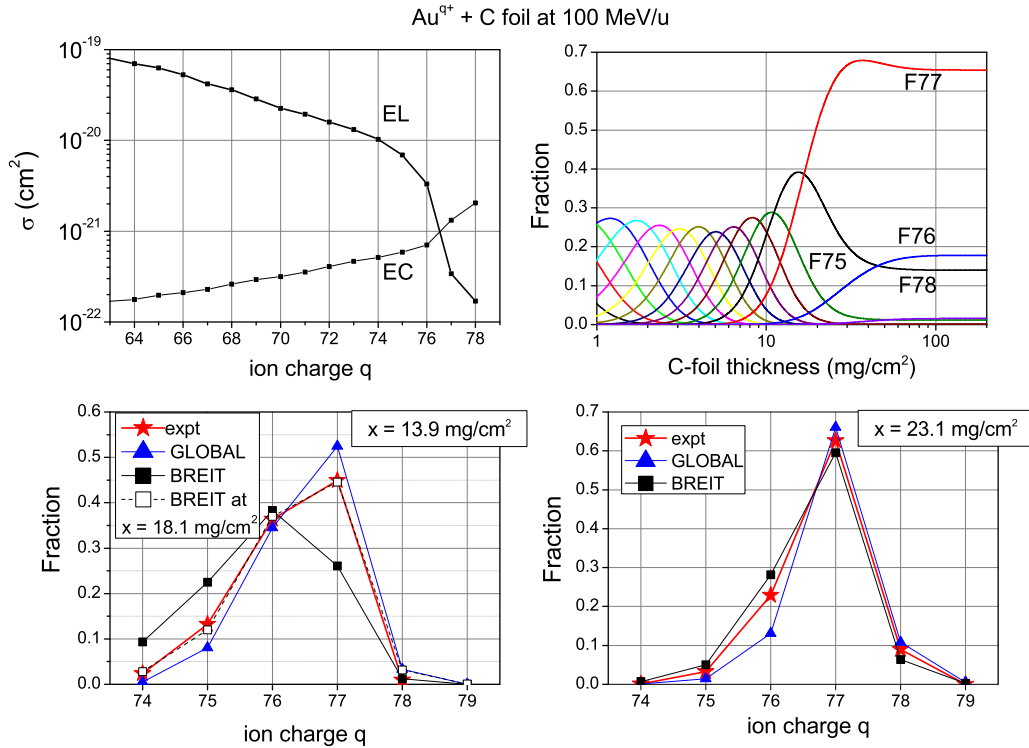


FIG. 3. Collisions of 100-MeV/u  $\text{Au}^{9+}$  ions with the C foil. Top left graph: calculated EL and EC cross sections from the present work. Top right graph: CSD of gold ions as a function of the C-foil thickness from the BREIT result. Bottom left and right graphs: CSDs at C-foil thicknesses  $x = 13.9$  and  $23.1$   $\text{mg}/\text{cm}^2$ , respectively, as a function of a gold-ion charge: stars, experiment [5]; triangles, the GLOBAL prediction [5]; squares, the BREIT result. In the bottom left graph, open squares show the BREIT result at C thickness  $x = 18.1$   $\text{mg}/\text{cm}^2$ .

larger thickness  $x = 18.1$   $\text{mg}/\text{cm}^2$  (open squares). The shift in the foil thickness can be explained by the fact that EL and EC cross sections, used in BREIT, are determined with an accuracy of 30%–50% at best; therefore, the accuracy of calculated CSD values is of the same order. For this reason,

calculated foil thicknesses  $x$  with a fixed set of the ion fractions are shifted compared to experimental  $x$  values. At carbon thickness  $x = 23.1$   $\text{mg}/\text{cm}^2$  (bottom right graph), both codes give results close to experiment. Finally, experimental probabilities [5] of creating  $\text{Au}^{77+}$  ions at C-foil thicknesses

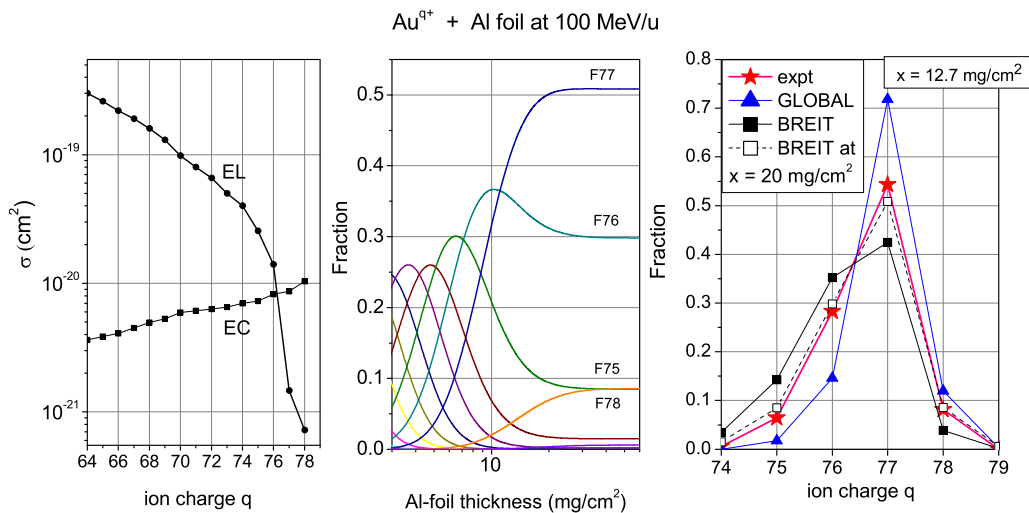


FIG. 4. Collisions of 100-MeV/u  $\text{Au}^{9+}$  ions with Al foil. Left: calculated EL and EC cross sections from the present work. Middle: charge-state distributions of gold ions as a function of Al-foil thickness from the BREIT result. Right: charge-state distributions at Al-foil thickness  $x = 12.7$   $\text{mg}/\text{cm}^2$  as a function of a gold-ion charge: stars, experiment [5]; triangles, the GLOBAL prediction [5]; squares, the BREIT result; dashed line with open squares, the BREIT result at Al thickness  $x = 20$   $\text{mg}/\text{cm}^2$ .

TABLE I. BREIT calculations of equilibrium characteristics for 100-MeV/u gold-ion beams stripped by C and Al foils: charge-state fractions  $F_{74}(\infty) - F_{79}(\infty)$ , foil thicknesses  $x_{\text{eq}}$  (in mg/cm<sup>2</sup>), and mean charges  $\langle q \rangle$  given by Eq. (11).

Equilibrium values	C foil with energy loss	C foil without energy loss	Al foil without energy loss
$F_{74}(\infty)$	0.0007	0.0006	0.015
$F_{75}(\infty)$	0.012	0.012	0.085
$F_{76}(\infty)$	0.14	0.14	0.30
$F_{77}(\infty)$	0.68	0.65	0.51
$F_{78}(\infty)$	0.16	0.18	0.086
$F_{79}(\infty)$	0.013	0.016	0.006
$\langle q \rangle$	77.04	77.01	76.57
$x_{\text{eq}}$	80	80	35

$x = 13.9$  and  $23.1$  mg/cm<sup>2</sup> are 45% and 63%, respectively, while the BREIT code predicts a maximal probability of 68% at  $x \approx 35$  mg/cm<sup>2</sup>.

The top right graph of Fig. 3 shows the CSD calculations, performed without accounting for the energy-loss effect; however, this effect can be estimated by the BREIT code. The ATIMA code [19] predicts 15% energy loss at equilibrium carbon thickness  $x_{\text{eq}} = 80$  mg/cm<sup>2</sup>, meaning an outgoing ion energy of 85.4 MeV/u instead of the incoming one of 100 MeV/u, which is quite a big difference. In fact, the ATIMA code predicts an energy loss of 4% for 100-MeV/u gold ions in carbon foil at  $x = 23.1$  mg/cm<sup>2</sup>, which is close to the experimental value of 3.74% [5].

In the interval 85–100 MeV/u, EL cross sections decrease 10% (see Fig. 1), while EC cross sections increase about 1.5 times. To calculate the fractions with energy loss included, the carbon thickness of 80 mg/cm<sup>2</sup> was divided into six layers, so that in each layer EC cross sections were considered constant within 25%. Consequently, the BREIT-calculated output fractions from one layer were used as the input values for the next one and so on. As a result, the influence of the energy loss on the charge-state fractions in this case is found to be quite small: the calculated fractions  $F_q(x)$  with the energy loss accounted for are about 12% larger than those without it.

Calculated equilibrium fractions  $F_q(\infty)$  of gold ions are given in Table I together with equilibrium charges  $\langle q \rangle$  and foil thicknesses  $x_{\text{eq}}$ . Results for Al foil, considered below, are also given in Table I. The equilibrium charge  $\langle q \rangle$  is calculated according to its definition:

$$\langle q \rangle = \sum_q q F_q(\infty). \quad (11)$$

For other cases considered further in this work, the energy losses, estimated with the ATIMA code, are found to be less than 10%, and therefore, CSD calculations are performed without the energy-loss effect.

### B. Al foil

Results for stripping 100-MeV/u gold ions by Al foil are given in Fig. 4. The present calculations of EL and EC cross sections are shown in the left graph, and the charge-state fractions  $F_q(x)$ , obtained with the BREIT code, are shown in

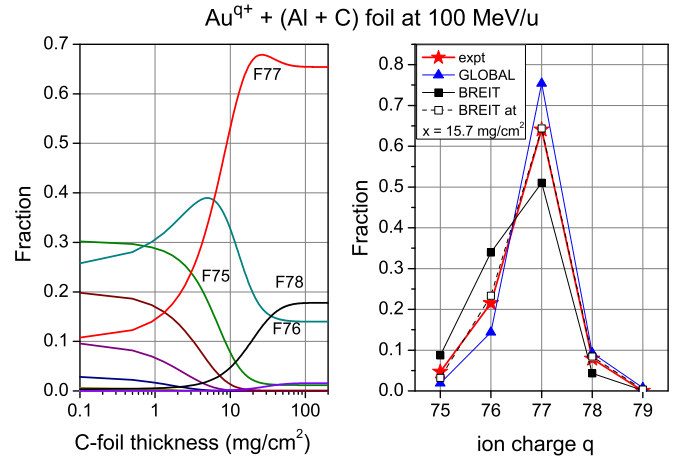


FIG. 5. Collisions of 100-MeV/u  $\text{Au}^{9+}$  ions with [6.4 mg/cm<sup>2</sup> Al + 9.24 mg/cm<sup>2</sup> C] foil. Left: charge-state fractions of gold ions in C foil after passing 6.4 mg/cm<sup>2</sup> thickness in Al foil for the BREIT result. Right: charge-state distributions of gold ions after passing [6.4 mg/cm<sup>2</sup> Al + 9.24 mg/cm<sup>2</sup> C] foil: stars, experiment [5]; triangles, the GLOBAL prediction [5]; squares, the BREIT result; dashed line with open squares, the BREIT result at C thickness  $x = 15.7$  mg/cm<sup>2</sup>.

the middle graph. The middle graph shows that the maximal value of the  $F_{77}$  fraction ( $\sim 52\%$ ) for Al foil is lower than that for C foil ( $\sim 68\%$ ), but the equilibrium thickness in Al foil is smaller than that for C foil (see Table I).

A nonequilibrium distribution of gold ions at Al thickness  $x = 12.7$  mg/cm<sup>2</sup> is given in the right graph of Fig. 4, showing a comparison of the RHIC experimental data with the GLOBAL and BREIT results. The BREIT calculations are very close to experimental data at higher Al thickness  $x = 35$  mg/cm<sup>2</sup> (open squares) for the same reason as in the case of C foil considered above. As a result, the experimental probability to create  $F_{77}$  fraction using an Al-foil stripper at thickness  $x = 12.7$  mg/cm<sup>2</sup> is 54%. The BREIT code predicts a maximal probability of 51% at  $x \geq 19.7$  mg/cm<sup>2</sup>, as shown in the middle graph.

### C. Al + C foil

Figure 5 shows results for stripping 100-MeV/u gold ions with a double-layer (Al + C) foil. This stripper, consisting of 6.4 mg/cm<sup>2</sup> of Al and 9.24 mg/cm<sup>2</sup> of C materials, was used at RHIC [5] as one of the candidates for obtaining He-like  $\text{Au}^{77+}$  ions with the largest probability.

The left graph shows the BREIT CSD in the C layer after ions pass through the Al layer that is 6.4 mg/cm<sup>2</sup> thick. In calculations, the gold-ion fractions in Al foil at  $x(\text{Al}) = 6.4$  mg/cm<sup>2</sup> are used as initial fractions for C foil at its thickness  $x(\text{C}) = 0$ . As expected, the calculated equilibrium fractions with (Al + C) foil coincide with those using only C foil (see the top right graph of Fig. 3 and Table I) because equilibrium charge-state fractions do not depend on the initial charge states of the incident ions (see [1,2,20]).

The right graph of Fig. 5 shows experimental and calculated fractions in C foil at  $x(\text{C}) = 9.24$  mg/cm<sup>2</sup> thick after exiting the Al foil at  $x(\text{Al}) = 6.4$  mg/cm<sup>2</sup>. The experimental  $F_{77}$  fraction is lower than that calculated by the GLOBAL code

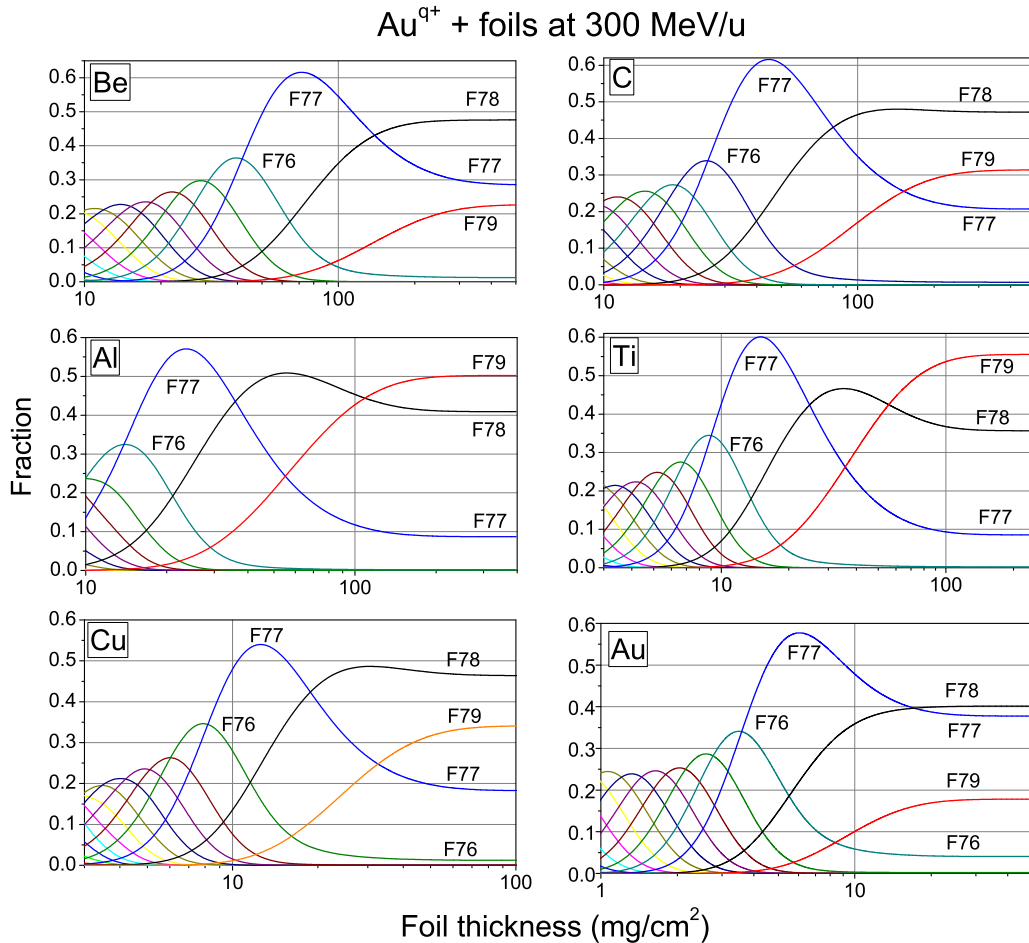


FIG. 6. Calculated charge-state fractions of 300-MeV/u gold ions stripped by foils from Be to Au (atomic numbers from  $Z = 4$  to  $Z = 79$ ) for the BREIT result. The foil materials are indicated in the top left corners of the graphs.

and higher than that found with the BREIT code; the BREIT results at higher C-foil thickness  $x(C) = 15.7 \text{ mg/cm}^2$  (open squares) are close to experimental data.

Using (Al + C) foil, the experimental maximal value  $F_{77}^{\max} \approx 64\%$  was obtained at RHIC [5]. The BREIT code predicts the same value,  $F_{77}^{\max} = 64\%$ , but for a double-layer foil with  $x = 6.4 \text{ mg/cm}^2$  Al +  $15.7 \text{ mg/cm}^2$  C.

Comparing three foils used at RHIC, C, Al, and (Al + C), the maximum output ( $\approx 64\%$ ) for the required fraction of Au<sup>77\*</sup> ions was experimentally obtained for C foil at  $x = 23.1 \text{ mg/cm}^2$  and for ( $6.4 \text{ mg/cm}^2$  Al +  $9.24 \text{ mg/cm}^2$  C) foil, both in the nonequilibrium regime.

The double-layer (Al + C) foil, used at RHIC, is 1.5 times thinner than the C foil, leading to different energy losses: 2.6% for the double-layer foil and 4.1% for the C foil. This means that the use of many-layer foils can be more effective for the energy-loss problem than foils made from one material. The BREIT code predicts 68% for the maximum probability to create Au<sup>77\*</sup> ions using C foil at  $x = 35 \text{ mg/cm}^2$  with 6.2% energy loss, estimated using the ATIMA code [19].

## V. STRIPPING GOLD IONS AT 300 MEV/u

The BREIT calculations for the CSDs of 300-MeV/u gold ions stripped by foils made from light (Be,  $Z = 4$ ) to

heavy (Au,  $Z = 79$ ) materials are shown in Fig. 6. The aim of this investigation is to find the gold-ion fractions with the maximum ion charge and the maximum probability (density).

One can see from Fig. 6 the strongly pronounced peaks of  $F_{77}$  fractions for He-like ions at the nonequilibrium thicknesses for all strippers considered. These peaks reach up to 60% probability, which is much higher than those in the equilibrium regime. Similar features of  $F_{77}$  fractions were observed experimentally in many papers, where different projectiles (C, Ar, Si, Ar, etc.) were stripped in C foils from low-charged ions up to the bare nucleus (see, e.g., [4,21–23]). The effect of extra-large fractions of He-like ions is also known from investigations of laser-produced plasmas, created in interaction of subpicosecond laser pulses with the target material [24].

The appearance of strong peaks of  $F_{77}$  fractions at nonequilibrium thicknesses can be explained in terms of the mean free path of gold ions in the foil. In Sec. III (Figs. 1 and 2), a big difference between EL cross sections of Li- and He-like gold ions is found, which actually constitutes the main reason for the specific behavior of  $F_{77}$  fractions.

Let us make some simple estimates, considering stripping gold ions by Be foil, as shown in Fig. 6. The ionization process of Au<sup>q+</sup> ions in a foil is characterized by a mean free path  $\lambda(q)$

TABLE II. Calculated equilibrium charge-state fractions  $F_{75}(\infty) - F_{79}(\infty)$ , foil thicknesses  $x_{\text{eq}}$  in (mg/cm<sup>2</sup>), and mean charges  $\langle q \rangle$  of 300-MeV/u gold ions, stripped by foils from Be to Au, for the BREIT result. The maximal nonequilibrium fractions of H-like ( $F_{78}$ ) and He-like ( $F_{77}$ ) gold ions are also given with corresponding foil thicknesses. The maximal fraction values are indicated in bold.

	Foil					
	Be	C	Al	Ti	Cu	Au
Data	Z = 4	Z = 6	Z = 13	Z = 22	Z = 29	Z = 79
$F_{75}(\infty)$	1.9e-4	1.1e-4	1.3e-5	3.3e-5	3.7e-4	0.002
$F_{76}(\infty)$	0.012	0.0071	0.0017	0.0025	0.012	0.041
$F_{77}(\infty)$	0.28	0.21	0.087	0.086	0.18	0.38
$F_{78}(\infty)$	0.48	0.47	0.41	0.36	0.46	0.40
$F_{79}(\infty)$	0.23	0.31	0.50	<b>0.56</b>	0.36	0.18
$\langle q \rangle$	77.9	78.1	78.4	78.5	78.1	77.7
$x_{\text{eq}}$	400	300	250	120	70	30
$F_{78}(\text{max})$	0.48	0.47	<b>0.51</b>	0.47	0.48	0.40
$x$	200	150	60	34	31	20
$F_{77}(\text{max})$	<b>0.62</b>	<b>0.62</b>	0.58	0.60	0.54	0.58
$x$	70	43	24	15	12	6.1

(in cm):

$$\lambda(q) = 1/[N_T \sigma_{\text{EL}}(q)], \quad (12)$$

where  $N_T$  is the foil material density (in atoms/cm<sup>3</sup>) and  $\sigma_{\text{EL}}(q)$  is EL cross section (in cm<sup>2</sup>). For this case one has  $N_T(\text{Be}) = 1.24 \times 10^{22} \text{ cm}^{-3}$  and, from Fig. 1,  $\sigma_{\text{EL}}(q) = 2.0 \times 10^{-21}$ ,  $1.0 \times 10^{-21}$ ,  $2.2 \times 10^{-22}$ , and  $1.2 \times 10^{-22} \text{ cm}^2$ , for  $q = 75, 76, 77$ , and  $78$ , and the corresponding  $\lambda$ -values are  $\lambda(75) = 4.0 \times 10^{-3}$ ,  $\lambda(76) = 8.0 \times 10^{-3}$ ,  $\lambda(77) = 0.037$ , and  $\lambda(78) = 0.067 \text{ cm}$ , respectively.

For the Be foil, the fraction  $F_{77}$  reaches its maximum at thickness  $x = 70 \text{ mg/cm}^2$ , i.e., at  $x = 0.04 \text{ cm}$ . This means that for the foil thickness of  $0.04 \text{ cm}$ , all fractions with a mean-free path  $\lambda < 0.04 \text{ cm}$  have already decreased, and the fractions with  $\lambda(q) \geq 0.04 \text{ cm}$  are close to their maximum, as is seen in the graph with Be foil. Certainly, this is an approximate explanation, but it helps us to understand the sharp growth of fractions for He-like ions. From Fig. 6 it follows that the largest  $F_{77}$  fraction can be obtained using Be and C foils at thicknesses  $x = 70$  and  $43 \text{ mg/cm}^2$ , respectively.

Another interesting feature, following from Fig. 6, is the creation of *bare* gold ions with maximum probability in the equilibrium regime or close to it. As the target atomic number increases, the  $F_{79}$  fraction first increases from  $F_{79} = 0.23$  for the Be foil, reaches its maximum of  $0.56$  for the Ti foil ( $Z_T = 22$ ), and then decreases to  $0.18$  for the Au foil. Therefore, the Ti foil ( $Z_T = 22$ ) seems to be the best one to get the maximal fraction with  $56\%$  for gold bare ions at  $300 \text{ MeV/u}$ .

Some predictions can also be made for the  $F_{78}$  fraction of H-like gold ions. For all foils, the  $F_{78}$  fractions do not exceed the level of  $0.4\text{--}0.5$ , and the optimal stripper is the Al foil, the use of which leads to the maximal production  $F_{78} = 51\%$  at  $x = 60 \text{ mg/cm}^2$ . The BREIT results of CSDs for stripping at  $300 \text{ MeV/u}$  are summarized in Table II, where the equilibrium fractions, the mean charges, and the foil thicknesses are given

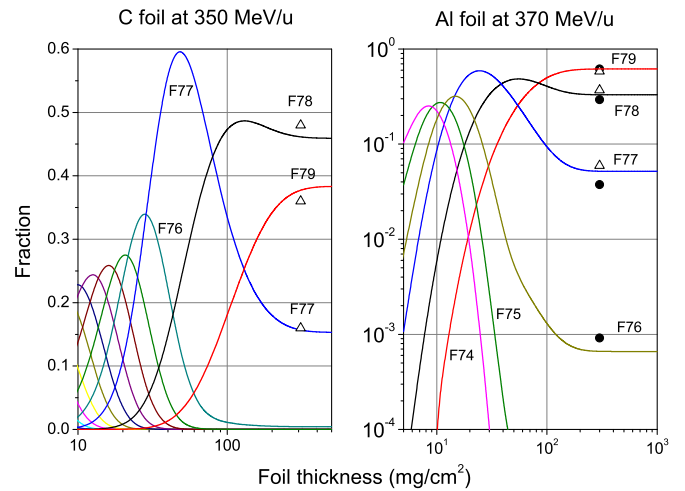


FIG. 7. Charge-state fractions of gold ions in collisions with C foil at  $350 \text{ MeV/u}$  and Al foil at  $370 \text{ MeV/u}$ : open triangles, the GLOBAL result; solid circles, experiment (both triangles and circles are from [4] for equilibrium thicknesses); curves, the BREIT result.

together with maximal nonequilibrium fractions of H- and He-like ions and corresponding foil thicknesses. The maximal fraction values are marked in bold.

## VI. STRIPPING GOLD IONS IN THE $350 \text{ MeV/u}$ TO $10 \text{ GeV/u}$ ENERGY RANGE

Figure 7 shows charge-state distributions of gold ions stripped by C foil at  $350 \text{ MeV/u}$  (left panel) and Al foil at  $370 \text{ MeV/u}$  (right panel) as a function of a foil thickness, where the BREIT results are compared with experimental data and GLOBAL calculations for the equilibrium fractions  $F_q(\infty)$  from [4]. The present results are in good overall agreement with both experimental and theoretical data [4]. Again, the fraction  $F_{77}$  of He-like gold ions has a pronounced maximum

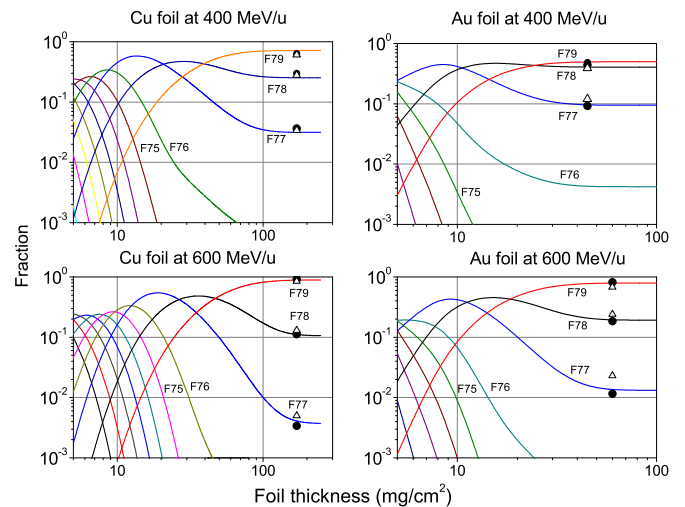


FIG. 8. Charge-state fractions of  $400\text{--}600\text{-MeV/u}$  gold ions in collisions with Cu and Au foils: solid circles, experiment; open triangles, the GLOBAL result (both circles and triangles are from [4] for equilibrium fractions); solid curves, the BREIT result.

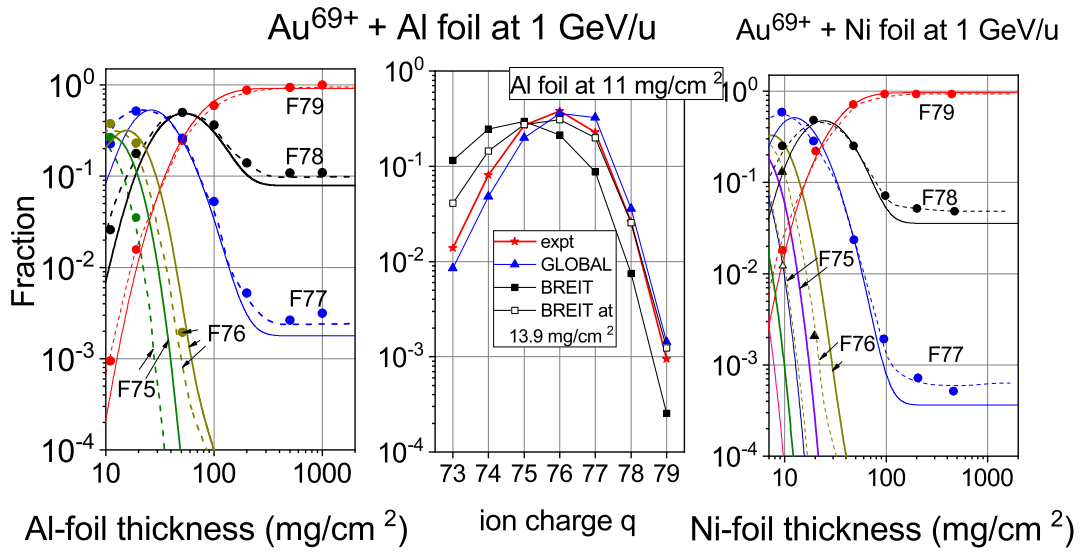


FIG. 9. Collisions of 1-GeV/u gold ions with Al and Ni foils. Left: charge-state distributions of incident  $\text{Au}^{69+}$  ions stripped by Al foil: solid circles, experiment [4]; dashed curves, the GLOBAL result [4]; solid curves, the BREIT result. Middle: charge-state distributions of incident  $\text{Au}^{69+}$  ions at  $x = 11 \text{ mg/cm}^2$  thickness in Al foil: stars, experiment [4]; triangles, the GLOBAL result [4]; solid squares, the BREIT result; open squares, the BREIT result at  $x = 13.9 \text{ mg/cm}^2$ . Right: charge-state distributions of gold ions stripped by Ni foil: solid circles, experiment [4]; dashed curves, the GLOBAL result [4]; solid curves, the BREIT result.

at nonequilibrium thickness due to the difference in the EL cross sections of Li- and He-like ions, leading to different mean-free-path values (see Sec. V).

A comparison of the BREIT calculations with experimental and calculated data [4] for CSDs of gold ions with Cu and Au foils at 400 and 600 MeV/u is given in Fig. 8, showing good agreement of the BREIT and GLOBAL calculations with experimental data for the equilibrium fractions.

The CSDs of relativistic gold ions are of interest for a new NICA project [6]. For planning experiments at the NICA collider, information about the efficiency to create bare gold

ions (fraction  $F_{79}$ ) is required at energies of 400–600 MeV/u after the first stripper.

From a recent work [7] and Fig. 8 it follows that the maximal ion fraction  $F_{79}$  can be obtained at 600 MeV/u in the equilibrium regime: using Cu foil with thickness  $x_{\text{eq}}(\text{Cu}) \approx 160 \text{ mg/cm}^2$  to obtain probability  $F_{79} \approx 90\%$  (bottom left graph) and using Au foil with  $x_{\text{eq}}(\text{Au}) \approx 60 \text{ mg/cm}^2$  to obtain probability  $F_{79} \approx 80\%$  (bottom right graph).

Charge-state distributions of 1-GeV/u gold ions stripped by Al and Ni foils are shown in Fig. 9 as a function of foil thickness. The left graph shows charge-state distributions in

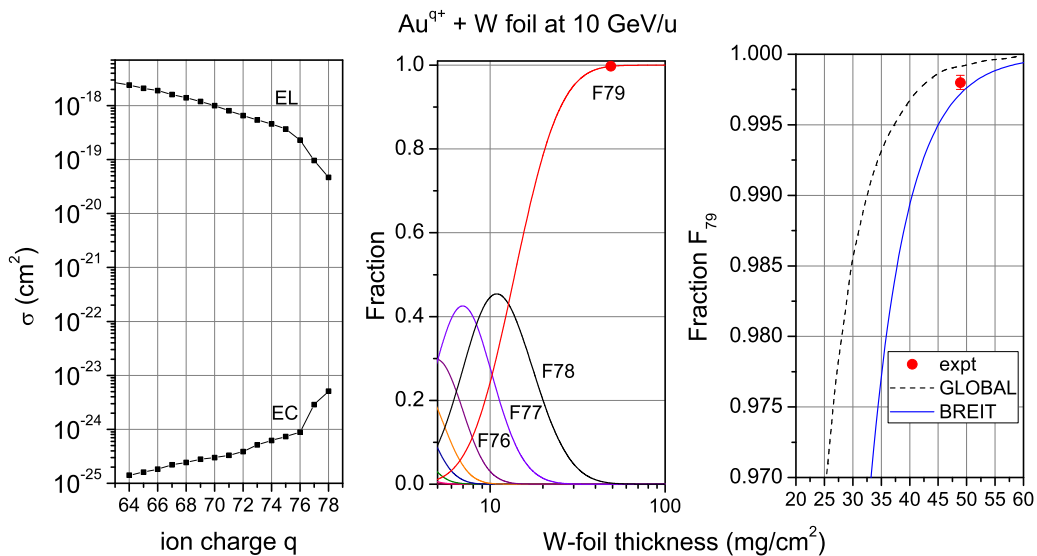


FIG. 10. Collisions of 10-GeV/u gold ions with W foil. Left: calculated EL and EC cross sections for the present result. Middle: charge-state distributions of gold ions as a function of Ni-foil thickness: solid circle, experiment [5]; solid curves, the BREIT result. Right: dependence of the  $F_{79}(x)$  fraction of bare gold ions as a function of W-foil thickness: solid circle, experiment [5]; dashed curve, the GLOBAL prediction [5]; solid curve, the BREIT result.



Al foil, calculated by BREIT (solid curves) and the GLOBAL (dashed curves) codes in comparison with experimental data [4]. All data are, on average, in good agreement, except for small Al thicknesses  $x < 30 \text{ mg/cm}^2$ . This difference at  $x = 11 \text{ mg/cm}^2$  is shown in the middle panel for ions with charges  $q = 73\text{--}79$ . At larger Al thickness  $x = 13.9 \text{ mg/cm}^2$ , the BREIT calculations roughly reproduce experimental data. As was pointed out before, the main reason for this fact is most likely related to the high uncertainties of the calculated EL and EC cross sections used in the BREIT code. The right graph of Fig. 9 presents results at 1-GeV/u energy for Ni foil. At Ni thicknesses  $x > 30 \text{ mg/cm}^2$ , there is good agreement between experiment, GLOBAL, and BREIT results, but at lower thickness, again, the disagreement is quite substantial.

Figure 10 displays EL and EC cross sections and charge-state distributions for 10-GeV/u gold ions stripped by W foil. The left graph shows the present calculations of the cross sections. In this case, NRC cross sections are negligible compared to the REC values. Charge-state distributions calculated by the BREIT code are shown in the middle graph. The energy loss at equilibrium thickness  $x_{\text{eq}} \approx 50 \text{ mg/cm}^2$ , calculated by the ATIMA code, is negligible. The solid circle is the experimental point for the fraction  $F_{79} = 0.489$  of bare gold ions at  $x = 0.998 \pm 0.0005 \text{ mg/cm}^2$  [5]. The right graph shows the dependence of charge-state fractions for bare gold ions as a function of W-foil thickness, obtained with the GLOBAL estimate [5] (dashed curve) and BREIT code (solid curve) in comparison with the experimental point. The difference between two theoretical calculations in this energy range is within 2%.

## VII. CONCLUSION

Charge-state fractions of relativistic gold-ion beams stripped by carbon and metallic foils are calculated by the BREIT code solving the balance rate equations with given electron-loss and electron-capture cross sections. Good overall agreement of the present data with available experimental and theoretical results is found in the energy range considered. The results demonstrate the reliability and good accuracy of the computer codes used for calculations of charge-changing cross sections, required for BREIT as input data. Finally, the following conclusions can be made:

(1) Detailed knowledge of charge-state dynamics of relativistic ion beams passing through solid foils allowed us to find the optimal conditions for the creation of H-like, He-like, and bare gold-ion fractions with the maximal charge or probability.

(2) The influence of the ion-beam energy loss on the CSDs of gold ions was found to be rather small: less than 15% at energies considered.

(3) Stripping accelerated heavy ions using multilayer (double-layer) foils holds special interest. Although these foils do not change the equilibrium charge-state distribution and the corresponding mean charge, determined by the element in the second layer, they can reduce the beam energy losses due to the shorter thickness of the double-layer foil compared to that with only one layer.

## ACKNOWLEDGMENT

The authors are grateful to Yu. Litvinov (GSI) for valuable discussions and remarks on the manuscript.

- 
- [1] R. D. Betz, Charge states and charge-changing cross sections of fast heavy ions penetrating through gaseous and solid media, *Rev. Mod. Phys.* **44**, 465 (1972).
- [2] P. Sigmund, *Particle Penetration and Radiation Effects* (Springer, Berlin, 2014), Vol. 2.
- [3] I. Yu. Tolstikhina and V. P. Shevelko, Influence of atomic processes on charge states and fractions of fast heavy ions passing through gaseous, solid, and plasma targets, *Phys. Usp.* **61**, 247 (2018).
- [4] C. Scheidenberger, Th. Stöhlker, W. E. Meyerhof, H. Geissel, P. H. Mokler, and B. Blank, Charge states of relativistic heavy ions in matter, *Nucl. Instrum. Methods Phys. Res., Sect. B* **142**, 441 (1998).
- [5] P. Thieberger, L. Ahrens, J. Alessi, J. Benjamin, M. Blaskiewicz, J. M. Brennan, K. Brown, C. Carlson, C. Gardner, W. Fischer, D. Gassner, J. Glenn, W. Mac Kay, G. Marr, T. Roser, K. Smith, L. Snyderstrup, D. Steski, D. Trbojevic, N. Tsoupas, V. Zajic, and K. Zeno, Improved gold ion stripping at 0.1 and 10 GeV/nucleon for the Relativistic Heavy Ion Collider, *Phys. Rev. Spec. Top. Accel. Beams* **11**, 011001 (2008).
- [6] NICA, <http://nica.jinr.ru/>.
- [7] V. V. Borodich, O. I. Meshkov, S. V. Sinyatkin, I. Yu. Tolstikhina, A. V. Tuzikov, V. P. Shevelko, and N. Winckler, Dynamics of Charge States of Relativistic Gold Ion Beams Passing through Cu and Au Foils in the NICA Project, *Zh. Eksp. Teor. Fiz.* **156**, 419 (2019) [*J. Exp. Theor. Phys.* **129**, 349 (2019)].
- [8] N. Winckler, A. Rybalchenko, V. P. Shevelko, M. Al-Turany, T. Kollegger, and T. Stöhlker, BREIT code: Analytical solution of the balance rate equations for charge-state evolutions of heavy-ion beams in matter, *Nucl. Instrum. Methods Phys. Res., Sect. B* **392**, 67 (2017).
- [9] G. Baur, I. L. Beigman, V. P. Shevelko, I. Yu. Tolstikhina, and T. Stöhlker, Ionization of highly charged relativistic ions by neutral atoms and ions, *Phys. Rev. A* **80**, 012713 (2009).
- [10] V. P. Shevelko, I. L. Beigman, M. S. Litsarev, H. Tawara, I. Yu. Tolstikhina, and G. Weber, Charge-changing processes in collisions of heavy many-electron ions with neutral atoms, *Nucl. Instrum. Methods Phys. Res., Sect. B* **269**, 1455 (2011).
- [11] J. Eichler and T. Stöhlker, Radiative electron capture in relativistic ion-atom collisions and the photoelectric effect in hydrogen-like high-Z systems, *Phys. Rep.* **439**, 1 (2007).
- [12] I. Yu. Tolstikhina, I. I. Tupitsyn, S. N. Andreev, and V. P. Shevelko, Influence of relativistic effects on electron-loss cross sections of heavy and superheavy ions colliding with neutral atoms, *J. Exp. Theor. Phys.* **119**, 1 (2014).

- [13] V. P. Shevelko, O. N. Rosmej, H. Tawara, and I. Yu. Tolstikhina, The target-density effect in electron-capture processes, *J. Phys. B* **37**, 201 (2004).
- [14] H. A. Kramers, On the theory of X-ray absorption and of the continuous X-ray spectrum, *Philos. Mag.* **46**, 836 (1923).
- [15] A. Ichihara and J. Eichler, Cross sections for radiative recombination and the photoelectric effect in the K, L, and M shells of one-electron systems with  $1 \leq Z \leq 112$  calculated within an exact relativistic description, *At. Data Nucl. Data Tables* **74**, 1 (2000).
- [16] BREIT, <http://breit.gsi.de>.
- [17] BREIT documentation, <https://github.com/FAIR-BREIT/BREIT-DOC/blob/master/README.md>.
- [18] FAIR-BREIT/BREIT-CORE, <https://github.com/FAIR-BREIT/BREIT-CORE/tree/master/data/input>.
- [19] ATIMA, <https://web-docs.gsi.de/~weick/atima/atima14.html>.
- [20] N. Bohr and J. Lindhard, Electron capture and loss by heavy ions penetrating through matter, *Mat. Fys. Medd. K. Dan. Vidensk. Selsk.* **28**, 1 (1954).
- [21] Y. Sato, A. Kitagawa, M. Muramatsu, T. Murakami, S. Yamada, C. Kobayashi, Y. Kageyama, T. Miyoshi, H. Ogawa, H. Nakabushi, T. Fujimoto, T. Miyata, and Y. Sano, Charge fraction of 6.0 MeV/n heavy ions with a carbon foil: Dependence on the foil thickness and projectile atomic number, *Nucl. Instrum. Methods Phys. Res., Sect. B* **201**, 571 (2003).
- [22] Y. Sato, T. Miyoshi, T. Murakami, K. Noda, V. P. Shevelko, and H. Tawara, Penetration of 4.3 and 6.0 MeV/u highly charged, heavy ions through carbon foils, *Nucl. Instrum. Methods Phys. Res., Sect. B* **225**, 439 (2004).
- [23] T. Miyoshi, Penetration of fast positive ions through carbon foils: Analysis of density effects, Ph.D. thesis, Heavy Ion Medical Accelerator in Chiba (HIMAC), Toki, Japan, 2009.
- [24] O. Rosmej, GSI, 2009 (private communication).